

Urban Ozone Trends in Europe and the USA (2000-2021)

Beth S. Nelson^{1,2,*} and Will S. Drysdale^{1,2,*}

¹Wolfson Atmospheric Chemistry Laboratories, Department of Chemistry, University of York, Heslington, York, YO10 5DD, UK

²National Centre for Atmospheric Science, University of York, York, UK

*These authors contributed equally to this work.

Correspondence: Beth S. Nelson (beth.nelson@york.ac.uk) and Will S. Drysdale (will.drysdale@york.ac.uk)

Abstract. Trends in urban O₃ and NO₂ across Europe and the United States of America were explored between 2000-2021. Using surface monitoring site data from the TOAR-II and European Environment Agency databases, piecewise quantile regression (PQR) analysis was performed on 228 O₃ time series (144 European, 84 USA) and 322 NO₂ times series (245 European, 77 USA). The PQR analysis permitted 2 break points over the 23 year period to balance the intent to describe changes over a large time period, while still capturing the abrupt changes that can occur in urban atmospheres. Regressions were performed over quantiles ranging from 0.05 to 0.95 and indications of a slowing in the increase of high European O₃ levels was observed. In Europe, more trends were found to having an increasing O₃ trend between 2015-2021 compared with 2000-2004. The reverse was true in the USA, with a reduction in the number of sites with increasing O₃ trends when the same periods were compared. An analysis of the change points revealed a large proportion of sites in Europe, were the second change point in NO₂ switched from a positive to negative trend, occurred in 2020 (41/43 second change points in this year). This was attributed to a reduction in NO₂ due to the COVID-19 pandemic, however, in some cases these increasing trends have sustained beyond the recovery from restrictions.

1 Introduction

Tropospheric ozone (O₃) is a greenhouse gas and air pollutant harmful to human health, and plant growth (Fleming et al., 2018; Mills et al., 2018; Szopa et al., 2021). It is a secondary air pollutant, formed from the photochemical reactions of primary pollutants NO_x (NO + NO₂) and volatile organic compounds (VOCs). The chemistry of O₃ formation is non-linear and the effect of changing precursor concentrations can cause O₃ concentrations to increase or decrease depending on the photochemical regime found at a given location (Sillman et al., 1990; Sillman, 2002). Despite global successes in reducing primary pollutant emissions over the past few decades, global exposure to O₃ has been increasing throughout the 21st century. This is particularly observed in urban areas, where the vast majority of the global population live, projected to increase to 68% in 2050 from 55% in 2018 (UN, 2019). In a study of 12946 cities located worldwide, the average mean weighted O₃ concentration increased by 11% between 2000 and 2019, and the number of cities exceeding the WHO peak season O₃ standard increased from 89% to 96% (Malashock et al., 2022).

Due to the complexity of O₃ production, its trend direction, magnitude, and significance varies by location. A previous study
25 calculated trends in two O₃ metrics globally over the period of 2000 - 2014: 4th highest daily maximum 8-hour O₃ (4MDA8), and the number of days with MDA8 > 70 ppb O₃ (NDGT70) (Fleming et al., 2018). The study used data from 4801 global monitoring sites over this time period. For both of these metrics, downward trends were observed for most of the USA, and some sites in Europe. However, over the period of 2010-2014 (2,600 sites utilised), sites located in regions with the highest O₃ precursor emissions across North America, Europe and East Asia had the highest values in 4MDA8 and NDTG70. In North
30 America and Europe, this was particularly true for California and parts of southern Europe (Fleming et al., 2018).

Since the 1990s, a general downward trend in urban O₃ pollution has been observed in the United States (He et al., 2020). This reducing trend has been linked to stricter limiting regulations on the emissions of primary pollutants such as NO_x and VOCs. Although NO_x and VOC emissions in Europe have also been declining since the late 1980s, the trend in O₃ is less clear due to large inner-annual variation, driven by climate variability and the dispersion and transport of pollutants from other regions
35 (Jonson et al., 2006; Yan et al., 2018). Between 1995 and 2014, negative trends in the highest O₃ levels across urban sites in Europe were identified due to pollutant emission restrictions across Europe. However, increasing background levels, particularly in northern and eastern Europe, make it difficult to identify strong trends in urban O₃ when transboundary effects are considered (Yan et al., 2018). Despite this, a study of 93 suburban and urban sites across Europe identified notable enhancements in O₃ seasonal and annual means between 1995 - 2012, even with the continuous downward trend in anthropogenic
40 emissions across the continent (Yan et al., 2018).

Since these earlier studies, much of the literature focuses on the impact of the COVID-19 pandemic on air pollutant concentrations and trends (Lee et al., 2020; Shi et al., 2021; Grange et al., 2021; Sokhi et al., 2021). A study of eleven cities across the world, all of which implemented stringent lockdown measures in early 2020, captured sudden decreases in deweathered NO₂ concentrations, concurrent with sudden increases in O₃, in most locations (Shi et al., 2021). Another study employing
45 machine learning models to predict business-as-usual levels of pollutants, estimated that NO₂ concentrations were 32% lower than expected across 102 European urban background locations, whereas O₃ was 21% higher (Grange et al., 2021). It is highly likely that this global event has resulted in perturbations of both long-term NO₂ and O₃ trends, particularly in locations where lockdowns were stringent or lengthy.

This study examines the trends in urban O₃ and NO₂ using monitoring site data from 2020 - 2023. It employs quantile regression and change point detection to construct trends that capture the broad structure of a complex time series, while remaining explainable with consists statistics. Section 2 details the method used to create the trends, section 3.1 provides a high-level overview of the trends with section 3.1.1 focusing on the significance of the trends and highlighting features that are discussed in detail later on. Section 3.2 explores the information that can be gained from trends calculated over a range of quantiles and finally section 3.3 provides details on some of the features revealed earlier in the analysis.

55 **2 Methodology**

Hourly NO₂ and O₃ data were obtained for urban sites in the USA and Europe using the TOAR-II (Schröder et al., 2021) and European Environment Agency (EEA) (European Environment Agency, a, b) databases, using the r-packages toarR (Drysdale, 2024) and saqgetr (Grange, 2019) respectively. Those obtained from the EEA are categorised as urban traffic, urban background and urban industrial, while those from the TOAR database are categorised as urban and suburban. A full list of sites can be found in the supplementary information (SI table 1). TOAR-II data was retrieved between 2000-01-01 and 2021-12-31 (the latest available) and EEA data between 2000-01-01 and 2023-12-31, the latter being extended longer so the effects of the COVID-19 pandemic could be observed more clearly. Time series were required to have 90 % data coverage between 2000-01-01 and 2021-12-31 and retained time series were averaged to daily medians. Additionally, a small number of time series were removed following visual inspection - these are listed in SI table 2. This resulted in 228 O₃ time series (144 Europe, 84 USA), 322 NO₂ time series (245 Europe, 77 USA) and 126 O_x (NO₂ + O₃) time series (101 Europe, 25 USA).

Firstly, the time series were de-seasoned by calculating a monthly median climatology and subtracting this from the time series, producing an ‘anomaly’ time series. The NO₂ and O₃ anomaly time series were summed to produce O_x anomaly time series for sites that have both NO₂ and O₃ data available. Following this, several methods were defined to help describe trends. As the time series are non-linear Locally Estimated Scatterplot Smoothing (LOESS) was applied first. This method works by calculating many least squared fits over a moving weighted subset of the data – with this subset tuned based on the desired ‘smoothness’ of the result. In this case with a smoothing parameter (α) chosen as 0.5, which was determined by inspection to capture a balance of broad trends and medium-term non-linearity. LOESS works well for drawing the eye to features of the time series but does not allow for broad trends to be described numerically as the resulting slopes are changing continuously.

As such, quantile regression (QR) was used to define trends following the methodology in and using code provided by Chang et al. (2023). QR calculates a linear model that seeks to minimise the residuals with a defined proportion (τ) of the points above and below the fit line. For example, the scenario $\tau = 0.5$ splits the data 50:50 above and below the line. QR has the advantage of being insensitive to outliers and can be considered analogous to a “median” trend line. This is desirable for the longer-term trends being investigated here. The 1-sigma uncertainty for the QRs were calculated via a moving block bootstrapping method, where the data are subdivided into overlapping blocks that are $n^{1/4}$ points wide (or ~20 points for 20 years of hourly data). These blocks are shuffled to generate a new time series, and replicated 1000 times, and the standard deviation of these replicates calculated. This uncertainty was subsequently used in the determination of the p-value, providing a metric for the significance of the trends.

As described the QR will be a poor representation of a time series with non-linearities (hence first investigating the LOESS) as it will be using a single slope to define the whole trend across a complex time series. As urban concentration trends can change sharply (e.g. with policy intervention), the model requires freedom to represent these, therefore they were extended to use piecewise quantile regressions (PQR) with up to two break points (resulting in three trend lines). This allows the model to have some changes in the trends calculated, capturing sufficiently large-scale changes while still being able to describe a ~20 year time series with a small number of coefficients.

To determine what break points to use on each time series, 109 scenarios per time series defined by 1, 2 or 3 sequential QRs
90 were created, separated by break points occurring on the 1st of January in up to two years excluding the first and last 2 years
of a time series. In the cases where there were 2 break points, these were not allowed to occur within 5 years of each other.
The cases with 2 or 3 regressions were combined into a single PQR, (PQR1 and PQR2 respectively). All regressions were
calculated at $\tau = 0.05, 0.10, 0.25, 0.50, 0.75, 0.95$ and 0.95 .

To select ‘change points’ from the array of break points available, the model performance was evaluated via Akaike information criterion (AIC). The piecewise scenario with the minimum AIC at $\tau = 0.5$ were selected as the change points for a given time series. This is a decision that trades off between there being potential change points that only exist in cases where $\tau \neq 0.5$, and retaining the ability to relate trends to one another across all quantiles. As this study aimed to explore the trends across a large number of sites, defining the change points only using $\tau = 0.5$ is more appropriate, but future studies that reduce the number of time series could consider investigating how change points differ with τ in more detail.

100 Figure 1 demonstrates this process on a single time series. Change points could be assessed for their efficacy (i.e. is the effect of introducing a change point important, or has it only provided a trivial reduction in the AIC?) by comparing the QR and the best PQR1 and PQR2 cases, but as this does not substantively change the results presented here, this was not done and the PQR2 fits were determined to be the most appropriate in all cases.

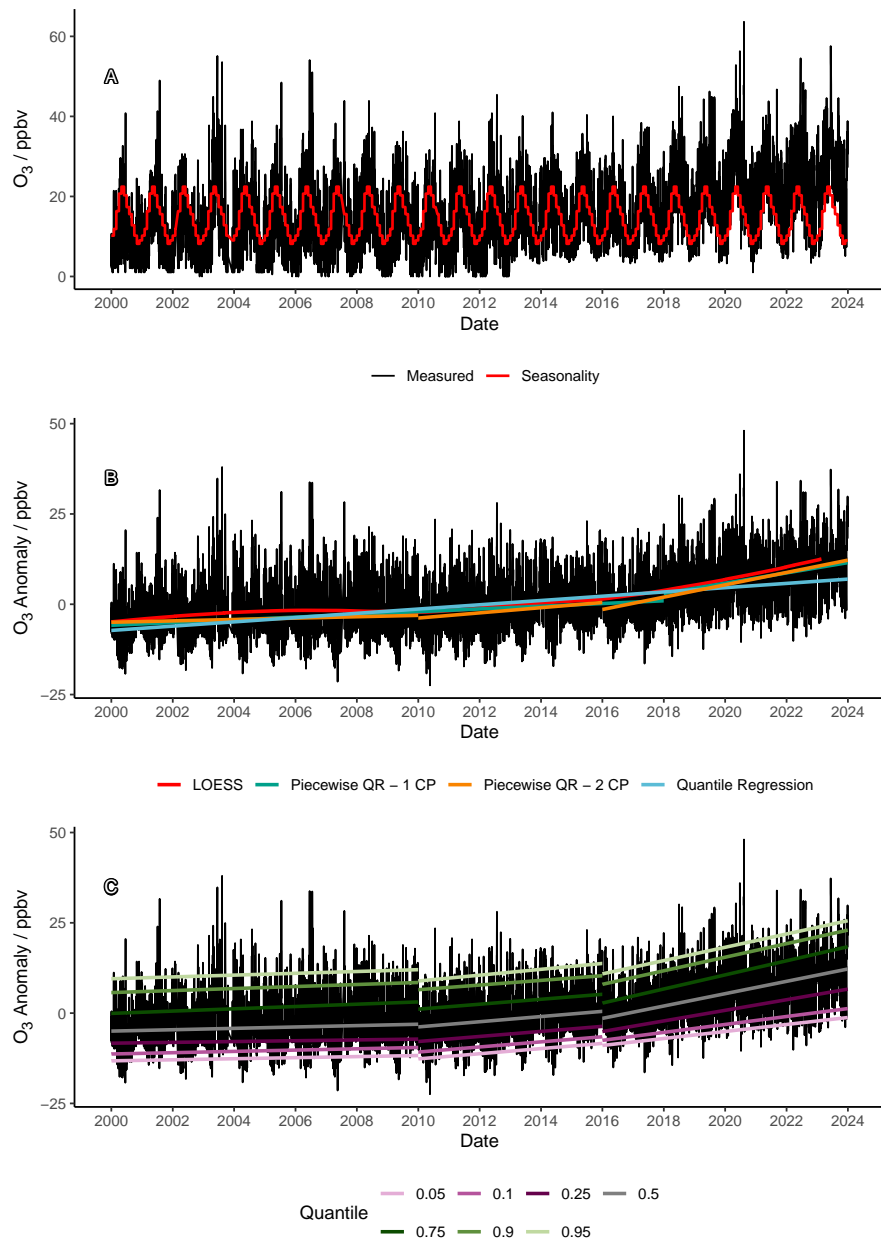


Figure 1. Example trend determination for an O₃ time series (London Bloomsbury - GB0566A). A - O₃ concentration time series (black) and monthly median climatology (red). B - Anomaly time series (black, concentration minus climatology) and 4 trend options, LOESS (red), QR (blue), PQR1 (green) and PQR2 (yellow). C - Anomaly time series (black) and PQR2 across $\tau = 0.05, 0.10, 0.25, 0.50, 0.75, 0.90, 0.95$. (purple to green)

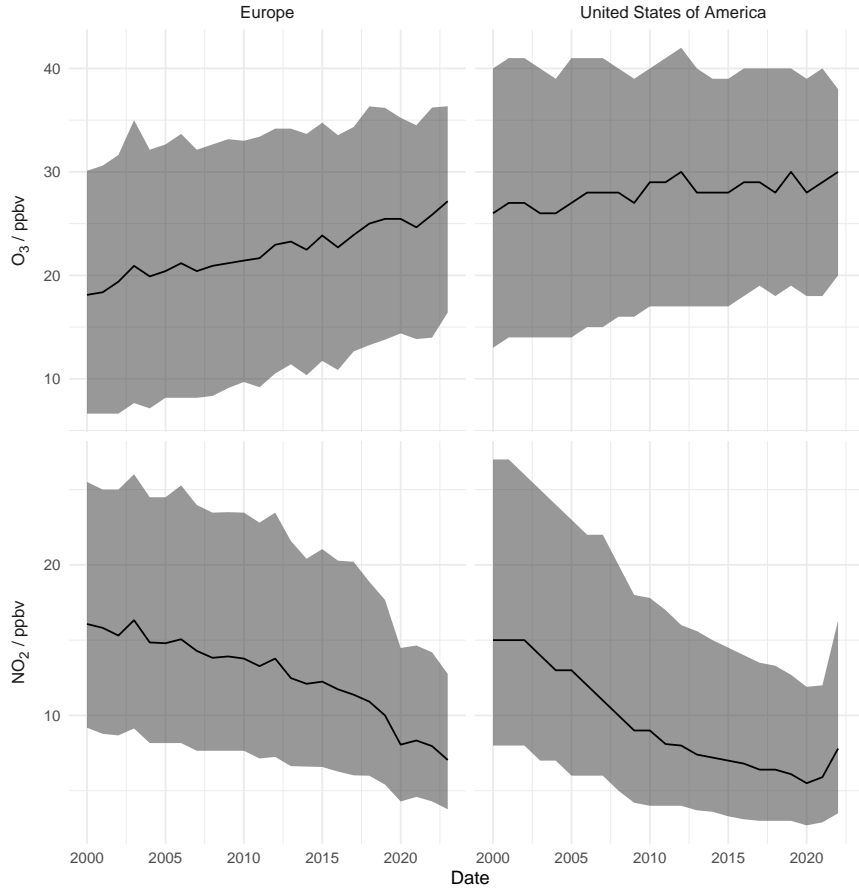


Figure 2. Median concentrations of O₃ (top) and NO₂ (bottom) across all sites in this study, separated into sites in Europe (left) and sites in the USA (right). Shaded regions represent the 25th and 75th percentiles.

3 Results and Discussion

105 To provide context for the subsequently calculated trends, figure 2 shows the annual median, 25 th and 75 th percentile concentrations of O₃ and NO₂ across all the urban sites used in this study. Europe shows median O₃ concentrations increasing from 18 ppb to 26 ppb between 2000 and 2019, and USA concentrations increasing, from 26 ppb in 2000 to 30 ppb in 2019. Both Europe and the USA show decreasing NO₂ over the same period (16 ppb to 10 ppb in Europe, 15 ppb to 6 ppb in the USA). The USA does see a return to increasing NO₂ concentrations after 2020, reaching 7.8 ppb in 2022. In section 3.3 evidence for 110 this increase is discussed.

The dataset that results from the application of the method described in section 2 has several degrees of freedom to bear in mind during discussion. For a given time series (one species at one site) there are two break points that are common for all the trend lines, and as there are 7 quantiles, this results in 21 slopes, each with an associated p-value. When comparing between

sites (or even species within a site) the change points can differ. This is necessary to capture the changing trends observed
115 at urban sites but does complicate describing them. For this discussion we have grouped the sites into those from Europe and those from the United States, though details on individual European countries are available in SI table 1. To aid in summarising, in some cases the results have been grouped into time periods of a few years – in these cases if a trend changes due to a change point both trends have been counted. For example, if between 2000 and 2004 a site were to go from increasing O₃ to decreasing O₃, this would be described as ‘between 2000 and 2004 there was one increasing O₃ trend and one decreasing O₃ trend’. In the
120 case where a site had a change point in 2003, but the trend remained increasing, this will be counted as one increasing trend. This has the benefit that no one category can count more than the number of available time series. In visualisation, both trends would be shown.

Trends have been collated into significance categories: $p \leq 0.05$ (high certainty), $0.05 < p \leq 0.10$ (medium certainty), $0.10 < p \leq 0.33$ (low certainty) and $p > 0.33$ (very low certainty or no evidence) based off of the guidance of Chang et al. (2023).
125 For the most part slopes where the p-value is > 0.33 are treated as ‘no trend’ regardless of their magnitude (generally we observe that as the magnitude of the trend decreases so does its significance), though sometimes are given with a direction when required by a visualisation.

3.1 Overview of Trends

The $\tau = 0.5$ trends of O₃ and NO₂ were examined and are presented on maps in figures 3 and 4.

130 In Europe, between 2000 and 2004 there were 108 trends where O₃ was increasing, and 41 where it was decreasing, 32 showed no trend. By 2015-2021, 123 had an increasing trend, 32 decreasing and 41 with no trend, indicating generally increasing O₃ concentrations across Europe. This is somewhat mirrored by the trends in NO₂, where in 2000-2004 69 trends were increasing, 181 decreasing and 59 with no trend, changing to 29 increasing, 241 decreasing and 39 with no trend by 2015-2021. This would suggest a general picture that urban locations in Europe are still on the VOC limited portion of the O₃ production
135 isopleth, and decreasing NO_x increases O₃ production, however, it is not quite as ubiquitous as this, as shown in 3.3.1 which discusses how O₃ responded to changing NO₂ following restrictions in 2020.

This contrasts with the USA, where in 2000-2004, there were 10 sites with increasing NO₂, and 0 sites increasing between 2005 and 2014, but in 2015-2021 17 sites had begun increasing in NO₂ again – though notably as seen from figure 4 these are different sites to those that were increasing at the beginning of the century. This increase in NO₂ is not clearly reflected
140 by the O₃ trends with 62 increasing, 23 decreasing and 22 showing no trend in 2000 – 2004 and 44 increasing, 34 decreasing, and 25 showing no trend in 2015-2021. A decreasing number of sites with a positive trend in O₃, suggests that the majority of decreasing NO₂ trends are slowing the increase in O₃. The counts of sites at all values of τ can be found in tables 2 and 3.

Across the entire study period, for O₃ in Europe, at sites with increasing trends the median slope was 0.36 ppb yr⁻¹, slightly lower than in the US, where they were increasing by 0.40 ppb yr⁻¹. For NO₂, the median rate of increase was the same in
145 Europe (0.36 ppb yr⁻¹), but higher at 0.71 ppb yr⁻¹ in the US. For decreasing trends, O₃ and NO₂ in Europe and the US were all similar, O₃ in Europe decreasing at -0.40 ppb yr⁻¹, (-0.36 ppb yr⁻¹) in the US and for NO₂ -0.39 ppb yr⁻¹ in Europe and -0.47 in the US. This information along with the 5 th and 95 th percentile (still at $\tau = 0.5$) are shown in table 1.

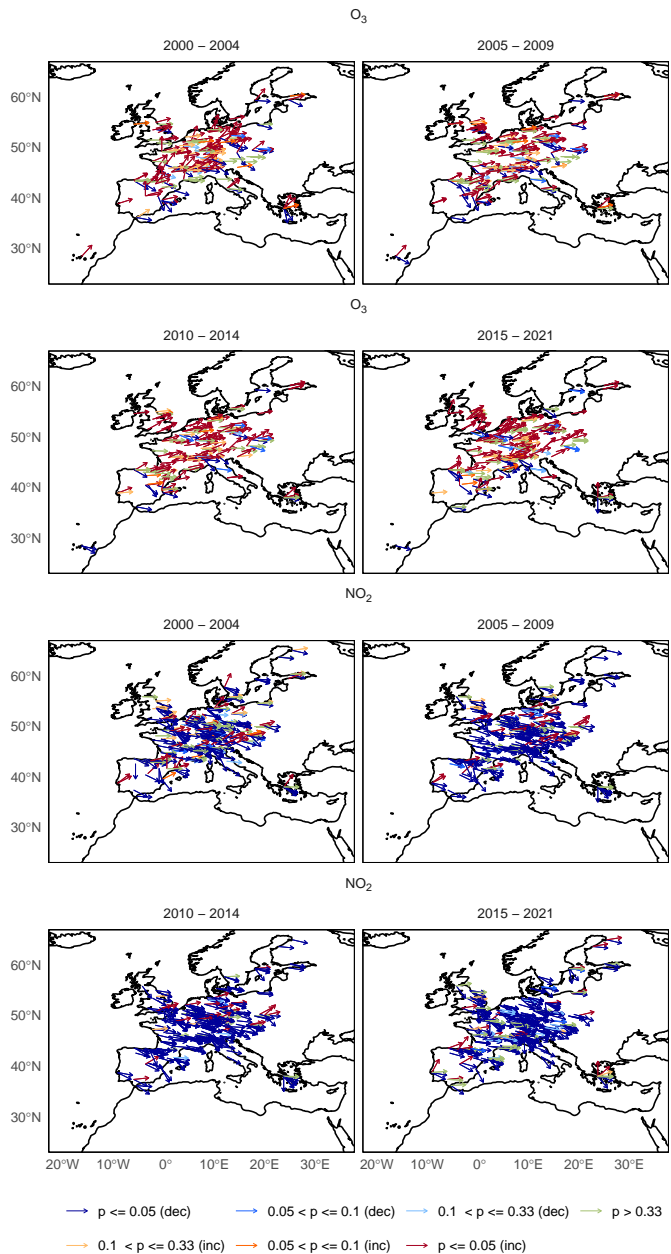


Figure 3. Summary of trends across Europe. Angle of arrow indicates magnitude and direction, with the following orientations: vertical up - $+2.5 \text{ ppb yr}^{-1}$, horizontal - 0 ppb yr^{-1} and vertically down - -2.5 ppb yr^{-1} . The few sites with absolute trends $> 2.5 \text{ ppb yr}^{-1}$ have been clamped to $\pm 2.5 \text{ ppb yr}^{-1}$. Colour indicates significance and direction, darkest colours being most significant ($p < 0.05$) and green the least ($p > 0.33$). Blues are decreasing trends and reds are increasing trends. The upper 4 plots show O_3 trends, and the lower 4 show NO_2 trends. Each group of 4 groups the trends into segments of the study period. If a change point occurs in a group an arrow for both trends is shown.

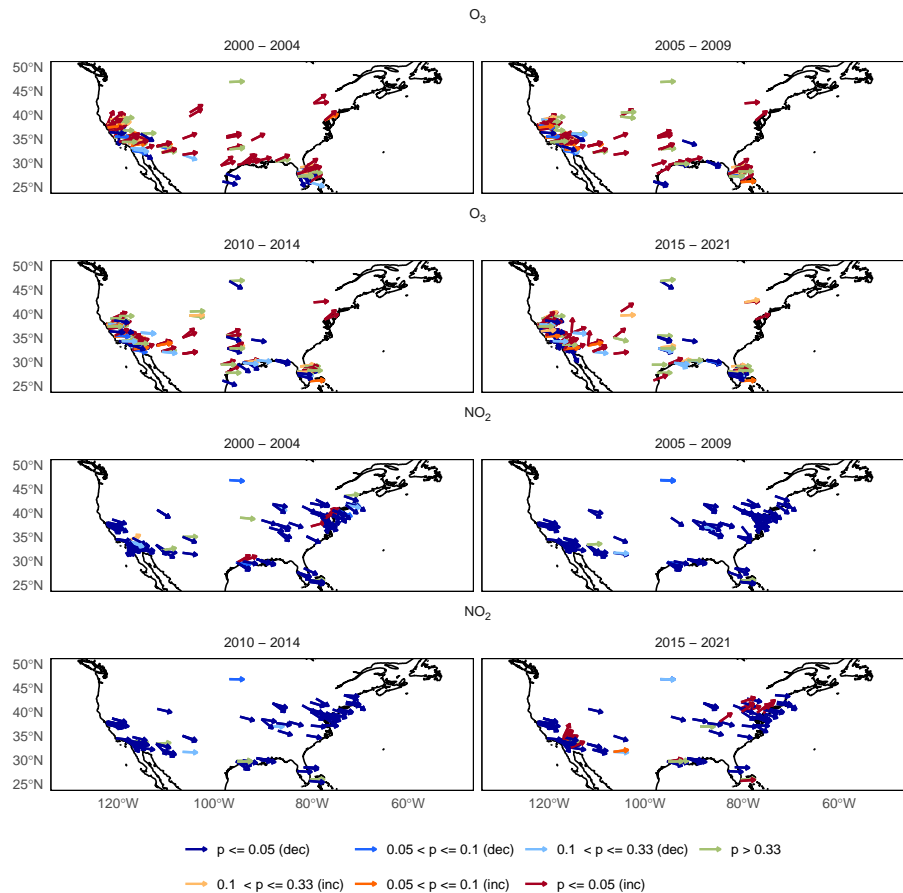


Figure 4. Summary of trends across the United States of America. Angle of arrow indicates magnitude and direction, with the following orientations: vertical up - +2.5 ppb yr⁻¹, horizontal - 0 ppb yr⁻¹ and vertically down - -2.5 ppb yr⁻¹. The few sites with absolute trends > 2.5 ppb yr⁻¹ have been clamped to ± 2.5 ppb yr⁻¹. Colour indicates significance and direction, darkest colours being most significant ($p < 0.05$) and green the least ($p > 0.33$). Blues are decreasing trends and reds are increasing trends. The upper 4 plots show O₃ trends, and the lower 4 show NO₂ trends. Each group of 4 groups the trends into segments of the study period. If a change point occurs in a group an arrow for both trends is shown.

Table 1. 5 th, 50 th and 95 th percentiles of the $\tau = 0.5$ slopes in Europe and the USA.

Species	Percentile	Slope / ppbv year ⁻¹					
		Europe			United States of America		
		Increasing	Decreasing	No Trend	Increasing	Decreasing	No Trend
O_3							
	5 th	0.09	-1.55	-0.11	0.11	-1.21	-0.14
	50 th	0.36	-0.40	0.00	0.40	-0.36	0.00
	95 th	1.46	-0.10	0.14	1.11	-0.09	0.13
NO_2							
	5 th	0.07	-1.32	-0.12	0.15	-1.36	-0.16
	50 th	0.35	-0.39	0.00	0.71	-0.47	0.00
	95 th	1.39	-0.10	0.11	1.35	-0.10	0.19
O_x							
	5 th	0.10	-1.16	-0.07	0.19	-1.41	-0.13
	50 th	0.41	-0.29	0.01	0.36	-0.31	0.00
	95 th	1.66	-0.06	0.19	1.22	-0.11	0.11

Table 2. Trends in O₃, NO₂ and O_x at sites in Europe in annual groups between 2000 and 2021 inclusive. If a site as a change point within a group, both slopes are added to the tally. Those classed as 'No Trend' are the slopes where p > 0.33

Species	τ	Increasing			Decreasing			No Trend				
		00 - 04	05 - 09	10 - 14	15 - 21	00 - 04	05 - 09	10 - 14	15 - 21	00 - 04	05 - 09	10 - 14
O₃												
0.05	112	114	119	123	23	21	15	24	45	46	33	47
0.10	114	119	124	127	26	23	16	23	36	36	26	44
0.25	107	110	115	127	32	30	19	30	40	42	31	41
0.50	108	108	115	123	41	40	23	32	36	36	30	41
0.75	104	99	107	120	40	38	24	36	38	44	39	45
0.90	99	93	104	111	43	43	23	32	44	50	41	53
0.95	93	84	96	101	44	43	25	33	50	60	53	61
NO₂												
0.05	59	48	31	23	169	197	223	242	80	54	33	67
0.10	68	45	31	27	169	205	230	243	73	51	26	50
0.25	66	43	29	30	183	217	236	243	59	33	18	49
0.50	69	42	27	29	181	224	238	241	59	32	14	39
0.75	73	44	22	22	175	220	237	242	60	34	18	35
0.90	73	43	20	17	166	218	238	241	72	40	21	39
0.95	78	44	18	15	157	207	236	241	83	50	29	42
O_x												
0.05	52	27	28	38	52	58	61	62	41	39	34	44
0.10	55	29	33	37	61	68	67	64	33	26	25	43
0.25	58	29	36	44	59	67	67	62	29	28	25	35
0.50	59	31	40	51	59	66	66	65	26	25	19	28
0.75	59	30	41	49	56	62	61	59	31	27	21	32
0.90	62	29	37	50	58	62	61	57	27	27	26	33
0.95	62	26	30	39	63	65	58	52	25	29	37	48

Table 3. Trends in O₃, NO₂ and O_x at sites in the United States of America in annual groups between 2000 and 2021 inclusive. If a site as a change point within a group, both slopes are added to the tally. Those classed as 'No Trend' are the slopes where p > 0.33

Species	τ	Increasing			Decreasing			No Trend				
		00 - 04	05 - 09	10 - 14	15 - 21	00 - 04	05 - 09	10 - 14	15 - 21	00 - 04	05 - 09	10 - 14
O₃												
0.05	68	64	54	49	10	11	18	20	28	23	30	38
0.10	71	67	55	50	9	9	19	24	25	18	27	32
0.25	69	63	54	47	13	10	25	32	24	21	28	27
0.50	62	57	46	44	23	19	33	34	22	24	29	25
0.75	55	50	41	39	25	24	41	40	30	28	23	24
0.90	42	38	35	36	30	30	43	41	36	35	31	28
0.95	36	33	29	31	37	36	44	39	34	33	31	34
NO₂												
0.05	11	3	3	10	70	74	68	60	16	10	14	24
0.10	11	3	5	12	74	77	69	62	13	6	10	20
0.25	13	3	4	14	71	75	74	67	10	4	5	17
0.50	10	0	0	17	74	77	76	72	6	2	5	7
0.75	9	0	0	16	75	77	77	74	5	1	3	6
0.90	6	0	0	9	75	77	77	74	15	0	2	14
0.95	7	0	0	7	74	77	76	74	15	3	3	17
O_x												
0.05	8	7	6	8	12	14	15	14	15	11	8	13
0.10	9	6	5	8	11	13	17	15	16	13	10	14
0.25	9	7	5	5	15	14	16	19	11	9	9	10
0.50	8	5	4	3	17	17	19	20	10	8	8	10
0.75	9	4	3	3	19	19	20	20	6	7	6	9
0.90	8	4	4	4	20	19	21	22	7	6	5	7
0.95	6	4	3	3	20	20	21	20	8	6	7	10

3.1.1 Significance of Trends

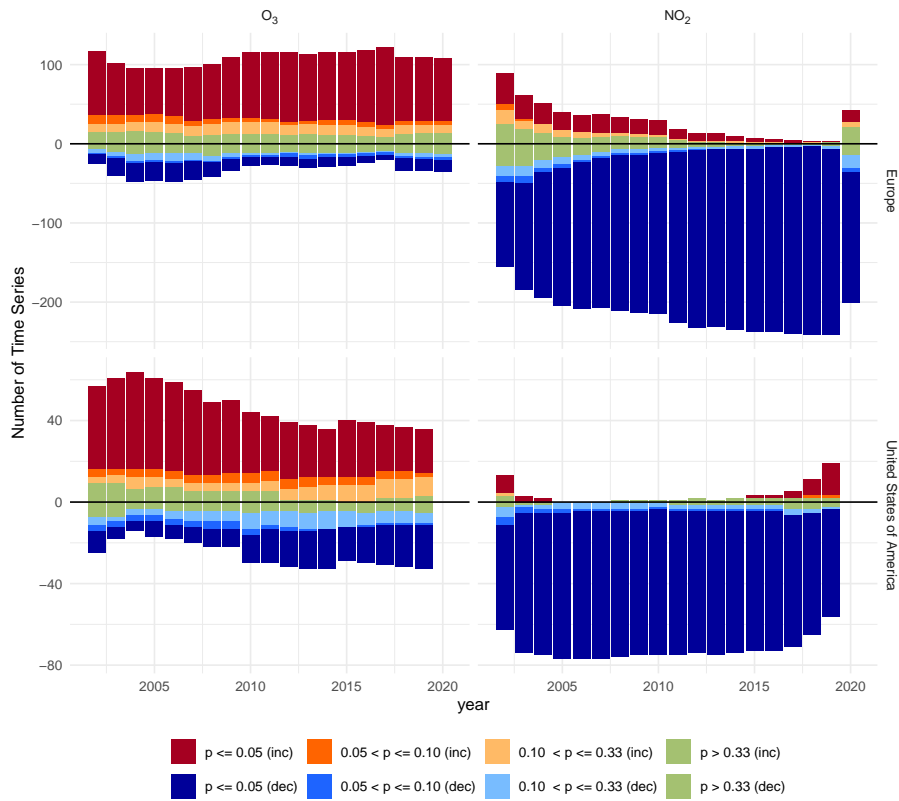


Figure 5. Time series of trends in O₃ (left) and NO₂ (right) for Europe (top) and the USA (bottom). Positive trends are contained in the bar above 0 and negative trends are contained in the bar below 0. Colour indicates significance and direction, darkest colours being most significant ($p < 0.05$) and green the least ($p > 0.33$). Blues are decreasing trends and reds are increasing trends. In this case trends with $p > 0.33$ have been sorted by their direction.

Figure 5 counts the trends by significance and direction per year. 2000, 2001 and 2021 onward in Europe and 2000, 2001, 150 2020 and 2021 onwards for the USA were excluded from this year on year analysis, as it is not possible to capture changing trends in these regions due to the limitations placed on where change points can occur as detailed in section 2.

This reveals the majority of trends are of high certainty. It also reinforces the observations from section 3.1, where both Europe and the US see O₃ increasing at number of sites, with there being proportionally more sites with a decreasing trend in the US. This additionally shows that the number of high certainty decreasing trends in O₃ has been present since ~2010, joined 155 by a slow decline in increasing trends.

For NO₂ the feature of some sites beginning to show increasing trends in the US is clear, with this pattern beginning in 2015-2016. Between 2000 and 2019 nearly all European sites moved to a trend of decreasing NO₂, however, this reversed for

several sites in 2020. This trend reversal can be attributed to the reduction in NO₂ concentrations in Europe which were a side effect of public health measures (Lee et al., 2020; Grange et al., 2021), and is discussed in more detail in 3.3.1.

160 3.2 Trends Across Quantiles

To investigate how the trends in urban O₃ are generally changing across quantiles in Europe and the USA, the distribution of slopes in each region was determined for each τ . This section necessarily needs to discuss two sets of quantiles referring to different calculations, as such τ is used to refer to the quantile associated with the quantile regression, and other references to quantiles are associated with the analysis of the distribution of slopes within a given τ .

165 The distributions at the start (year = 2000) and end (year = 2019) of the 20-year period were compared (Figure 6). Generally, across all values of τ , the interquartile range (IQR = 75th quantile minus 25th quantile) of the slope distributions in O₃ was greater in 2000 compared with 2019 ($\tau = 0.5$, IQR = 0.87 and 0.58 ppb yr⁻¹ for 2000 and 2019 respectively). This is particularly true for Europe, where a clear reduction in the higher τ O₃ slopes is observed between 2000 and 2019. For $\tau = 0.95$, a much larger proportion of the slopes were > 1.25 ppb yr⁻¹ in 2000 than 2019. For $\tau = 0.95$ in the USA, there is a reduction in the
170 number of slopes with very negative (< 1.00 ppb yr⁻¹) slopes between 2000 and 2019.

In Europe, the bulk of NO₂ slopes become more negative across all τ (Figure 6). However, in the USA, despite the majority of slopes being negative in both 2000 and 2019, there is still a proportion of slopes with positive slopes in 2019, not observed in the European distribution. This is particularly true for 0.5 >= τ <= 0.9. The IQR of the slope distributions was comparable between 2000 ($\tau = 0.5$, IQR = 0.50 ppb yr⁻¹) and 2019 ($\tau = 0.5$, IQR = 0.40 ppb yr⁻¹) for Europe, comparable to the reduction
175 in spread observed in the USA in 2019 ($\tau = 0.5$, IQR = 0.44 ppb yr⁻¹) compared to 2000 ($\tau = 0.5$, IQR = 0.57 ppb yr⁻¹).

Annual changes in τ slopes were used to evaluate how absolute urban O₃ mixing ratios and trends changed across Europe and the USA between 2000 and 2021. For both Europe and the USA, the cumulative sum of the annual median of the trends across all sites was calculated for each value of τ . This was followed by the subtraction of the 2000 value to get relative change since 2000. Using this analysis, Figure 7 shows the change in median O₃ and NO₂ mixing ratios since 2000. The median of
180 these results for Europe and the United States of America was then derived for each year and for each τ . From this, Figure 8 describes how the magnitude and direction of the trend line changes annually.

In both Europe and the USA, median trend-derived O₃ mixing ratios have generally increased between 2000 and 2021 (figure 7). This is most clearly observed in Europe, where all percentiles demonstrated a consistent increase in median O₃ across the two decades. Larger increases in O₃ were observed in the lower τ cases (+6.33 ppb, $\tau = 0.05$) compared to the higher τ cases
185 (+5.08 ppb, $\tau = 0.95$), indicating that the lowest ambient O₃ levels are continuing to increase while higher levels show some signs of reducing their rate of increase. The picture is more mixed in the USA. Similarly to Europe, the largest increases in median O₃ since 2000 were observed in the lower τ cases (+4.95 ppb, $\tau = 0.05$). In the $\tau = 0.50$ case, median O₃ increased to ca. +2.5 ppb by 2011 before plateauing between 2011 and 2021. In contrast, in the highest τ value cases, median O₃ was lower in 2021 than in 2000 (-0.76 and -0.60 ppb, $\tau = 0.90$ and 0.95 respectively). This suggests that higher ambient levels of O₃ have
190 reduced in magnitude since 2000, compared to lower ambient levels which are continuing to increase. In both Europe and the USA, median ambient NO₂ mixing ratios have reduced, with the largest reductions observed in the $\tau = 0.95$ case (-11.49 ppb

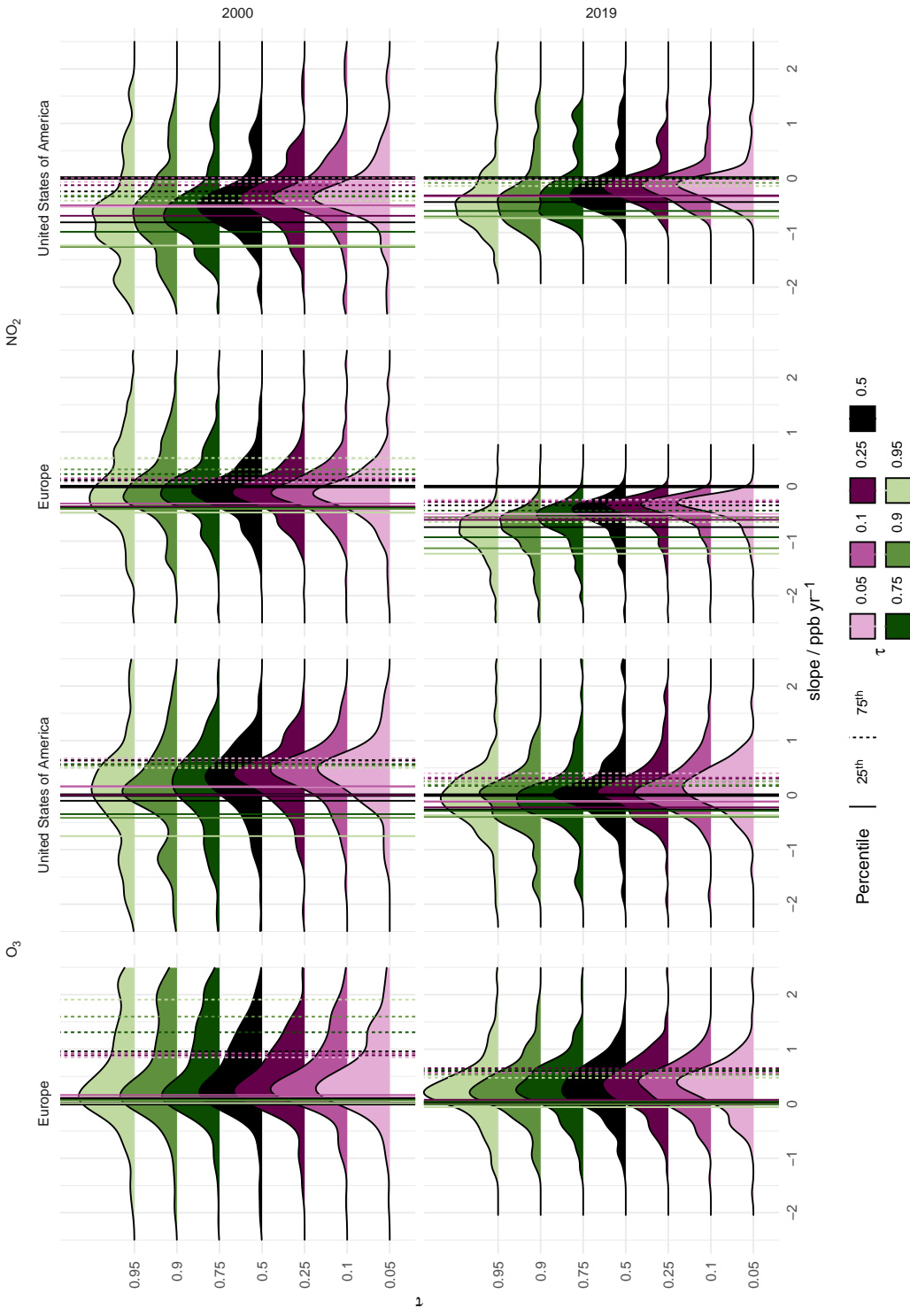


Figure 6. Slope density for NO_2 (left) and O_3 (right) for Europe (cols 1 and 3) and the USA (cols 2 and 4) in 2000 (top) and 2019 (bottom) for $\tau = 0.05, 0.1, 0.25, 0.5, 0.75, 0.9$ and 0.95

and -15.94 ppb for Europe and the USA respectively). Smaller reductions were observed in the $\tau = 0.05$ case (-4.48 and -5.78 ppb for Europe and the USA respectively).

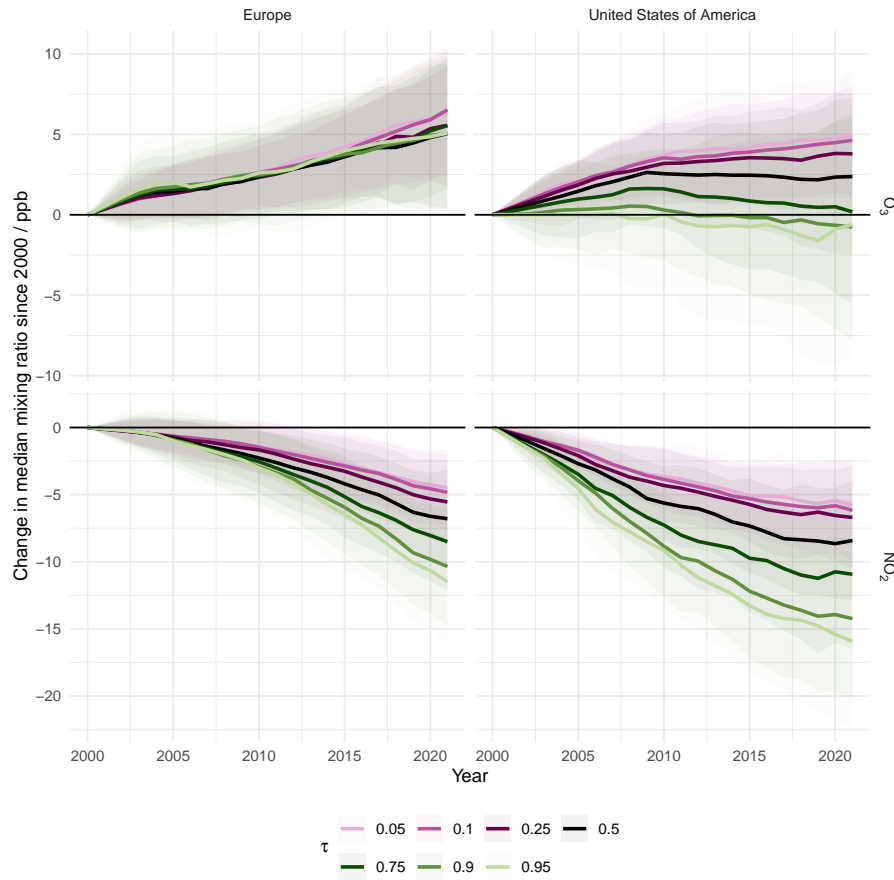


Figure 7. Absolute change in trend line-derived median NO_2 , O_3 and O_x mixing ratios for Europe and the USA, coloured by trend line percentile. The shaded region represents the median absolute deviation.

Taking a closer look at the annual magnitude and direction of the trends allows for a closer inspection of how O_3 and NO_2 trends have changed between 2000 and 2021 for each τ value (Figure 8). For Europe, all median O_3 trends were positive for 195 all τ values across all years. For higher τ values ($\tau = 0.75, 0.90$ and 0.95), the slope dropped sharply from ca. 0.54 ppb yr^{-1} to ca 0.07 ppb yr^{-1} ($\tau = 0.95$) between 2000 and 2004. A smaller decrease in slope was observed for the lower τ cases (from ca. 0.35 ppb yr^{-1} to 0.18 ppb yr^{-1} for the $\tau = 0.05$ case). From 2005 onward, the slope in the O_3 trend generally continued to increase up to 2021. In the lower τ cases, the median slope returned to 2000-2002 levels in 2021. For the higher τ cases, the 200 magnitude of the median slope was between ca. $0.29 - 0.46 \text{ ppb yr}^{-1}$ lower in 2021 than 2000. In the USA, a larger spread in the changing median slopes was observed between different τ values. Generally, and in contrast to Europe, the median slope in O_3 steadily decreased between 2000 and 2014, before plateauing between 2014 to 2021. For the lower τ values, the slope in

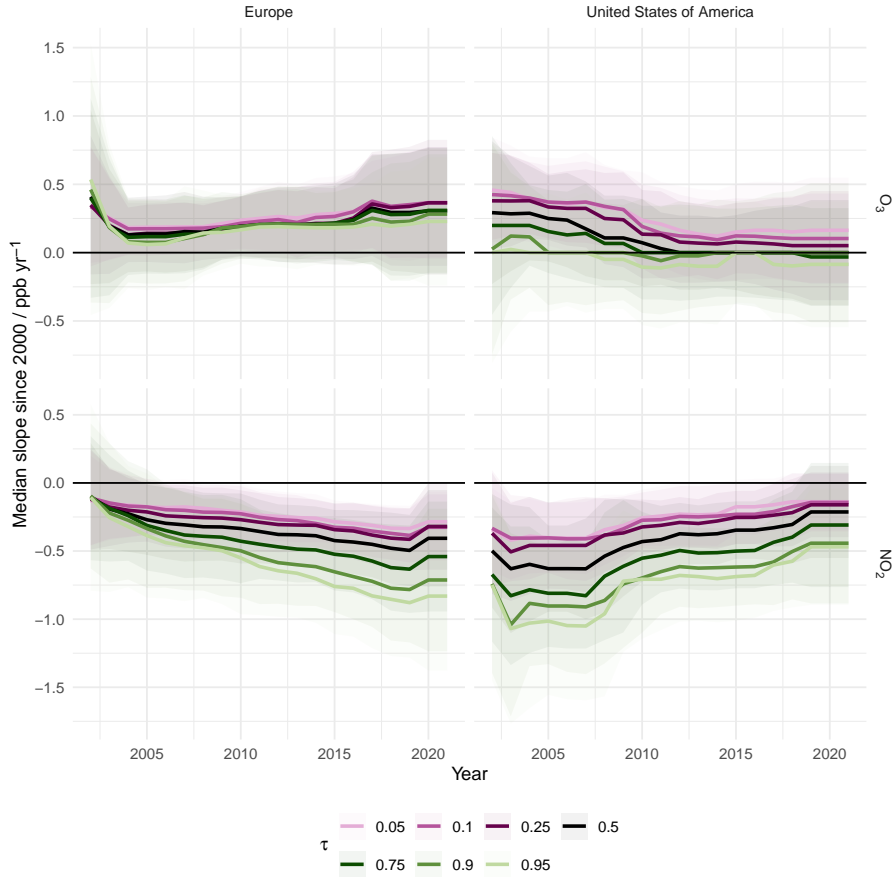


Figure 8. Median trend line slopes (ppb yr^{-1}) in NO_2 , O_3 and O_x for Europe and the USA, coloured by trend line τ value. The shaded region represents the median absolute deviation.

O_3 remained positive between 2000 and 2021, but reduced by ca. 0.34 ppb yr^{-1} between 2000 and 2014 ($\tau = 0.05$). Trends in the higher τ cases were positive at the beginning of the century, with a transition to a negative trend observed for $\tau = 0.75$ (in 2013), and $\tau = 0.90$ and 0.95 (both in 2007). In the $\tau = 0.50$ case, median trends in O_3 plateau around 0 ppb yr^{-1} from 2012, indicating no overall direction of trend.

Trends in NO_2 in Europe and the USA between 2000 and 2021 are also contrasting. In both Europe and the USA, median trends remain negative between 2000 and 2021, indicating NO_2 is decreasing in both cases, as observed in Figure 7. However, the direction of the trend is different in each region. In Europe, the slope of the trend is becoming increasingly more negative with time, particularly for the higher τ cases (reduction of ca. 0.72 ppb yr^{-1} for the $\tau = 0.95$ case). However, in the USA the negative trends are becoming increasingly more positive (or less negative) between 2000 and 2021 (0.29 ppb yr^{-1} higher, $\tau = 0.95$).

3.3 Spatio-temporal Distribution of Change points

The direction and magnitude of the change points in each location were investigated to identify locations where a change in direction of the trend (i.e. a negative to positive trend) occurs. In Europe, 21 sites observed a switch from a negative O₃ trend line to a positive one in the first change point. The biggest switches occurred in southern Europe, in Spain and Greece ($\Delta 3.28$ ppb in *gr0022a*, 2004). For a larger number of sites (41), mainly in central Europe, the first change point in O₃ switched from positive to negative, up to a maximum swing of 4.55 ppb (*fr31013*, 2003). In contrast, a larger number of sites observed a negative to positive switch (39) in the second change point, compared to a positive to negative switch (28). Eight of the top ten biggest switches from negative to positive in the second change point occurred in Spain and Italy ($\Delta 3.99$ ppb in *es0124a*), whereas the biggest switch from positive to negative showed no distinct spatial pattern. This suggests that generally across Europe, more trends in O₃ were switching from positive to negative in the first 5-10 years of the 21st-century, whereas more trends were switching from negative to positive between 2010-2021. In both decades, southern European sites showed the biggest changes in O₃ trend from negative to positive. Similarly to O₃, more sites showed a positive to negative trend (84) in NO₂ compared to negative to positive (28) for the first change point, with the largest change points again observed in Spain ($\Delta 3.25$ ppb, *es1453a*). A comparable number of sites showed changes in trend direction in the second change point, (43 negative to positive, and 33 positive to negative). The positive to negative trends were generally distributed around 2010-2014, whereas the vast majority of negative to positive switches occurred in 2020 (41 out of 43 sites). The cause of this switch in 2020 across Europe is discussion in further detail in section 3.3.1.

In the USA, a comparable number of directional switches in O₃ trend in the first change point occurred in the positive to negative direction (21), compared to negative to positive (17). The three largest magnitude trend changes from negative to positive occurred in Florida ($\Delta 2.43$ ppb, *15292*), with all of the ten highest magnitude cases in either Florida or California. Trends switching from positive to negative in the first change point scenario were smaller in magnitude, the biggest switch being in California ($\Delta 1.53$ ppb, *8197*), but with some noticeable contributions from the central states. The majority of second change points occurred between 2010-2019, though it is important to note that due to a lack of data availability, it is not possible for this analysis to pick out change points from 2020 onward in the USA dataset. In total, 14 sites switched from positive to negative, with a maximum change of $\Delta 2.25$ ppb (*8169*, 2019). A comparable number of sites (12) showed trends switching from negative to positive, with a maximum change of $\Delta 2.46$ ppb (*1959*, 2019). In the NO₂ dataset, there is only one site showing a switch from negative to positive in the first change point ($\Delta 1.30$ ppb, *1369*, 2008), compared to 13 sites showing a positive to negative switch. Of these 13 sites, the largest magnitude is in Virginia ($\Delta 2.99$ ppb, *15024*, 2003). In contrast, 19 sites show a switch in NO₂ trend from negative to positive after the second change point, with the biggest change in California ($\Delta 2.16$ ppb, *1206*, 2019), with only one site showing a switch from positive to negative ($\Delta 0.48$ ppb, *1369*, 2013).

Generally, the largest changes from negative to positive O₃ trends in the USA were in California and Florida in the first half of the 20 year period, with the reversal of this trend seen across California and Florida in the second change point. 8/14 and 4/14 of the sites showing a positive to negative transition in the second change point were located in California and Florida

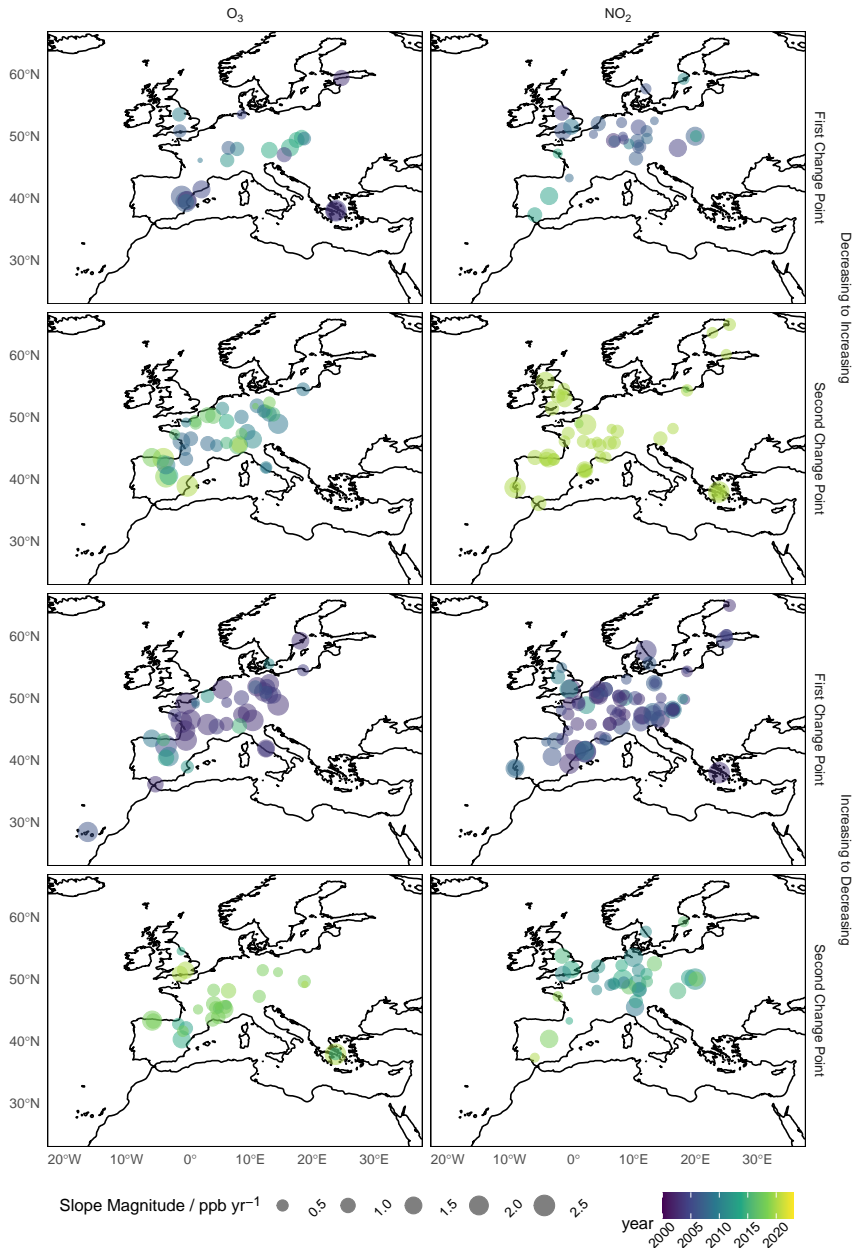


Figure 9. European sites with a change in direction of slope (O_3 - left, NO_2 - right) of the first (rows 1, 3) second (rows 2, 4) change points. The size of the slope is relative to the magnitude of the change in slope (slopes $> 2.5\ ppb\ yr^{-1}$ have been clamped), coloured by the year of the change point. Negative to positive change points (rows 1, 2) are presented separately to positive to negative change points (rows 3, 4).

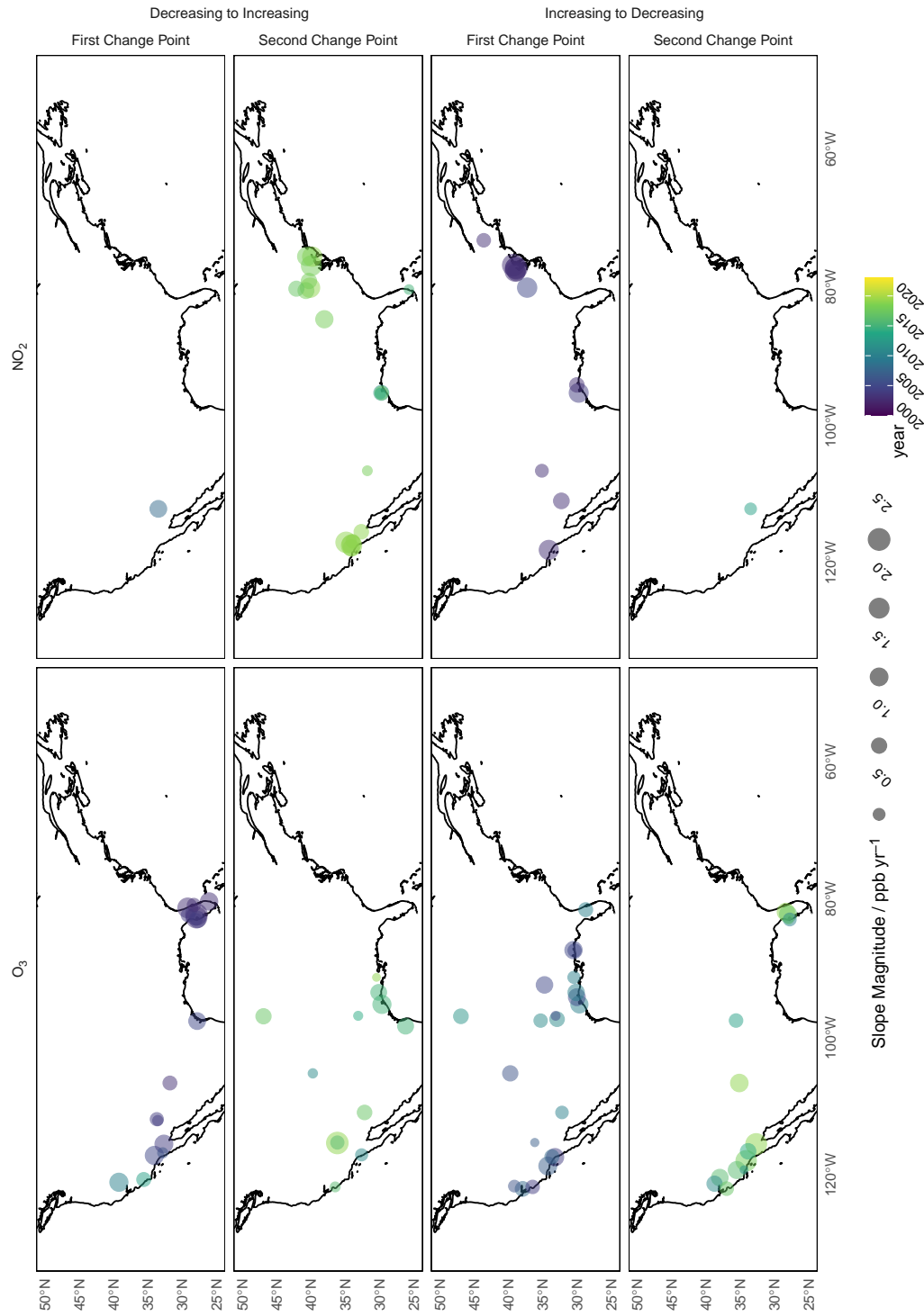


Figure 10. US sites with a change in direction of slope (O_3 - left, NO_2 - right) of the first (rows 1, 3) second (rows 2, 4) change points. The size of the slope is relative to the magnitude of the change in slope (slopes $> 2.5 \text{ ppb yr}^{-1}$ have been clamped), coloured by the year of the change point. Negative to positive change points (rows 1, 2) are presented separately to negative change points (rows 3, 4).

respectively. This is important, since a previous study highlighted that 4th highest daily maximum 8-hour O₃ (4MDA8) values between 2010-2014 were particularly high in California (Fleming et al., 2018).

To supplement this analysis, the 4MDA8 was calculated using the mixing ratio data for each site and slicing the fourth highest value on an annual basis. 4MDA8 is an important metric used by the US for determining compliance with the National Ambient Air Quality Standards for Ozone (Environment Protection Agency, 2015; Berrocal et al., 2014). To allow for comparison with previous studies, only the 6-month warm season (April - September) was used to calculate 4MDA8 values, which is a reasonable approach in the USA and Europe since the highest O₃ values are likely to occur in the warmest months.

Figure 11 shows how the 4MDA8 value varies between 2000, 2007, 2014 and 2021 in the USA. Across the US, 33 sites had a 4MDA8 >= 85 in 2000, compared to 19 in 2007 and 6 in 2014. In 2016 there was an up-tick to 10 sites with 4MDA8 values at this level. Of these 10 sites, all are located in California, compared to 20/33 Californian sites in 2000 and 18/19 in 2007. All 11 sites in 2021 with 4MDA8 >= 85 were located in California. This highlights that although fewer Californian sites are exceeding 4MDA8 >= 85 ppb with time over the 2-decade period, the Californian 4MDA8 "hotspot" identified in Fleming et al. (2018) is still present. The more general picture across the USA is that 4MDA8 values are coming down with time, particularly strongly in the central and Eastern portion of the USA but less successfully in the west.

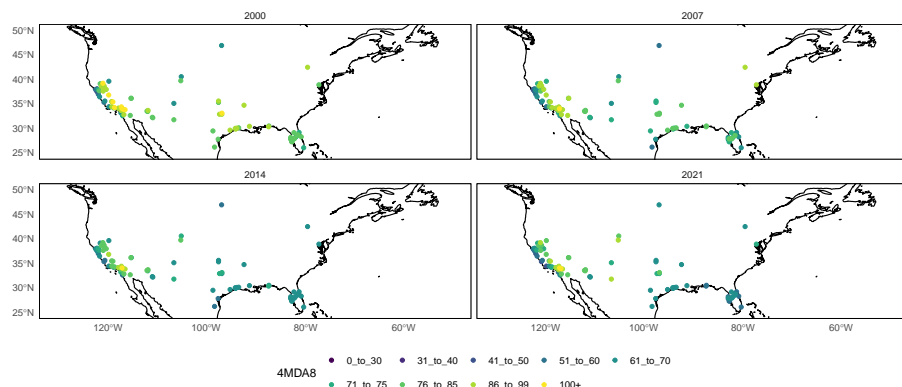


Figure 11. 4MDA8 values in ppb for sites in the United States in 2000, 2007, 2014 and 2021

Southern Europe, particularly Greece and Northern Italy, were also highlighted in Fleming et al. (2018) as being 4MDA8 hotspots. Figure 12 shows how the 4MDA8 values are changing between 2000, 2007, 2014 and 2021 across Europe. In 2000, there were 6 sites in which 4MDA8 >= 85 ppb. This slightly increased to 7 sites in 2007 before decreasing to 4 sites in 2014.

By 2021, no sites had 4MDA8 values exceeding 85 ppb. Since the measurement sites in this dataset are not evenly distributed across the USA and Europe, it is difficult to attribute high 4MDA8 values to particular states or countries. However, it was noticeable that a large proportion of the sites were 4MDA8 \geq 85 ppb were in Italy and Greece. In 2000 3/6 of high 4MDA8 sites were located in Italy, and 1/6 in Greece. In 2007, 3/7 were located in Italy and 1/7 in Greece; and in 2014 3/4 sites were located in Italy. Consistent with the Fleming et al. (2018) study, the southern European 4MDA8 hotspots are apparent throughout the 20-year period.

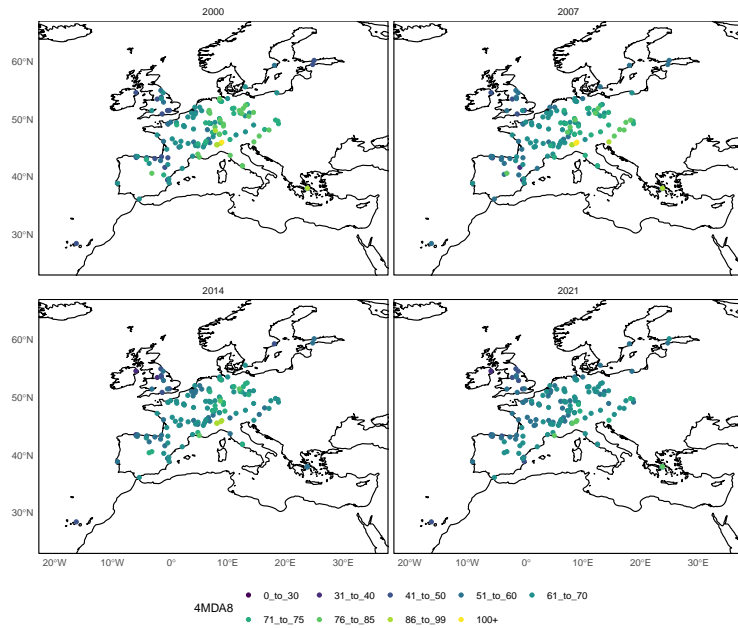


Figure 12. 4MDA8 values in ppb for sites in Europe in 2000, 2007, 2014 and 2021

3.3.1 2020 In Europe

As noted in section 3.1.1, in 2020 in Europe several sites switched from a long term decrease in NO₂ to increasing NO₂ again. The public health measures enacted due to the COVID-19 pandemic had the side effect of decreasing NO₂ concentrations due to reduced traffic emissions. The removal of these measures led to an increase in NO₂ mixing ratios as normal activities resumed, resulting in a positive trend in NO₂ concentrations up from their lowest during the restrictions. There are 42 sites that had a negative trend in 2019 and a non-negative trend in 2020. The 2019 trends ranged from 1.47 to -0.04 ppb yr⁻¹ and the 2020 trends ranged from 0.00 to 3.74 ppb yr⁻¹. There were two sites that already had non-negative trends (*fr25039* and *pl0048a*) by 2020, but neither were strong or significant ($p > 0.33$). The effect of this on O₃ concentrations at the sites is varied. 21 of the 42 sites also measured O₃, though only 3 (*es1038a*, *fr33120* and *gr0031a*) also had 2020 as one of the change points for the PQR. To compare the 2020 onwards trends, new PQRs for each site were selected by requiring the second change point

to occur in 2020, and then selecting where the first occurred on a time series by time series basis by minimising the AIC as
280 before. Furthermore, only sites where the resulting slope for the 2020 onwards O₃ trend had p values < 0.33 were selected. One final site (*gr0031a*) was removed as although it meets the data coverage criteria for the main analysis, its missing data is focused around 2019 and 2020 which has a strong influence on the trends derived. This led to 15 sites remaining for this case study. The resulting alternative trends for these sites are shown in figure 13. Additionally, as the focus is on sites with both NO₂ and O₃, O_x is displayed. If a site is under a VOC limited regime, the trend in O_x provides an indication whether any
285 changes in O₃ are only due to changes in NO₂, or other factors. Whether a change in NO₂ concentrations results in an increase or decrease in O₃ concentrations depends on the if a site is sensitive to locally produced O₃ (which an urban site, in general, would be expected to be), and what photochemical regime (NO_x or VOC limited) the site is under. For example, in a VOC limited regime, if NO₂ increases, O₃ decreases but O_x remains the same, the change in O₃ can be attributed to the change in NO₂. If NO₂ and O₃ increase, O_x will also increase, indicating a NO_x limited regime. 14 of the sites saw increasing O₃ with
290 increasing NO₂ between 2020 and 2023 - this is expected in NO_x limited regimes. Due to the need for both O₃ and NO₂ to be measured at both sites 13 of the sites were urban background and 2 were urban traffic, as O₃ is less frequently measured at traffic sites. Urban background sites are more likely to be under NO_x limited regimes as they are, by design, situated further from major roads, which are still a significant source of NO_x. This does not necessarily mean that urban areas in Europe are completely NO_x limited and will depend on the specific location as to whether an urban traffic or urban background site is
295 more representative of a location. At one urban traffic site (*es1529a*) has seen decreasing O₃ with increasing NO₂ over the same period. This is more indicative of a VOC limited regime, and is more similar to the overall trends seen across Europe in the 21st century, with more increasing O₃ trends in 2015-2021 than in 2000-2004.

The sites identified by this method do not appear to have resumed their pre-2020 trends, though this should be verified when sufficient data has been collected post-2020 where change points will have more freedom to occur. The pattern of sites
300 switching to an increasing trend in NO₂ will have varied effects on urban O₃ in Europe if they continue, though as background sites are designed to be more representative of residential areas, which make up a large portion of urban areas then it could be expected to see urban O₃ continue to increase.

3.3.2 Recent NO₂ in the USA

In the final years of the USA NO₂ dataset, an up-tick the number of positive NO₂ trends can be seen. From 2015 onwards there
305 is an increasing number of sites with this trend reaching 17 sites trends (16 high, 1 medium certainty) in 2021, up from 0 in 2014. Anomaly time series and trends of can be viewed in figure 14. Trends have reversed from -0.98 - -0.03 ppb yr⁻¹ to 0.1 - 1.78 ppb yr⁻¹. Unfortunately, only 4 of the 17 sites have concurrent measurements of O₃ so it is difficult to investigate this changing trend in NO₂ from the time series analysed in this study. Only one site (8169) O₃ trend has its original second change point occurring alongside its NO₂ increasing change point, so the same method has been applied as in 3.3.1 where the second
310 change point has been forced to occur in the same year as the NO₂ change point. Doing this reveals that sites 8169, 14386 and 15197 have reasonably significant (p = 0.01, 0.15, 0.002 respectively) O₃ trends after change point 2, when this change point is the same as that in NO₂. 8169 and 14386 have decreasing O₃ trends (-1.70 and -0.55 ppb yr⁻¹) with increasing NO₂ and 15197

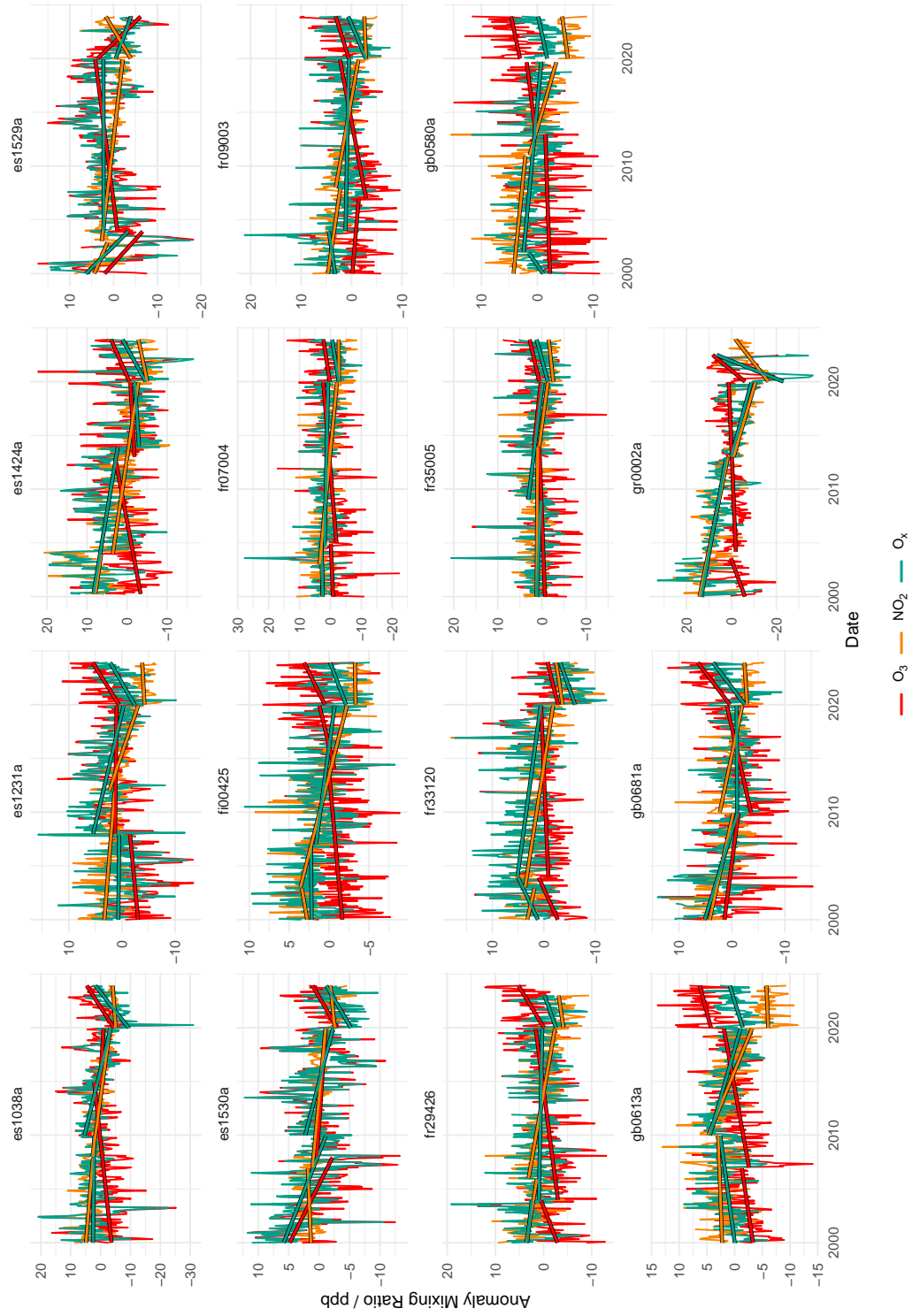


Figure 13. Sites in Europe that had decreasing NO_2 in 2019 but increasing NO_2 from 2020 onwards. Monthly averaged O_3 (red), NO_2 (orange) and O_x (green) anomaly are shown. O_3 and O_x trends differ from those presented elsewhere in the manuscript as the piecewise quantile regression where the second change point has been restricted to be in 2020.

saw increasing O₃ at 1.15 ppb yr⁻¹. These data suggest that the O₃ concentrations will be sensitive to this increase in NO₂, but without the co-located O₃ measurement it does not provide definitive information on the direction on any changes. Indeed
315 Jhun et al. (2015) note that reductions in NO_x suggested that the 99.9th quantile O₃ concentrations were also reduced between 1994 and 2010. While this study limits itself to the 95th quantile, there is some indication in figure 7 that there has been a small increase in high O₃ levels during the time increased NO₂ is observed.

4 Conclusions

Trends in urban O₃ and NO₂ were calculated from de-seasoned monitoring site data across both Europe and the USA. A
320 quantile regression analysis was utilised to assess long-term trends, while the method was extended with a piecewise approach allowed for some freedom to capture changes in a complex dataset, whilst being able to describe the trends with a small number of coefficients. In Europe, more sites were found to have an increasing O₃ trend between 2015-2021, compared to 2000-2004, with NO₂ trends showing the reverse effect (fewer sites increasing, and more decreasing in 2015-2021 compared to 2000-2004). This broadly suggests that a VOC-limited relationship for O₃ formation could be common across urban sites in Europe.

325 In the USA, the reverse is true, with a reduction in the number of sites with increasing O₃ trends in 2015-2021 compared with the 2000-2004 period, but with more sites with increasing NO₂ in 2015-2021 compared with 2000-2004. The majority of O₃ trends are positive and of high certainty ($p \leq 0.05$) in Europe across the 20-year period. This is also broadly true for the USA, but the proportion of sites showing this trend reduces with time, alongside an increase in the number of sites with high certainty negative trends in O₃ between 2010-2021. From these trends, the median (\pm median absolute deviation) change in O₃ over the
330 last two decades were calculated as 5.0 ± 4.6 ppb in Europe and 2.4 ± 4.9 ppb in the USA, with corresponding changes in NO₂ as -6.8 ± 3.6 and -8.4 ppb.

An exploration of the τ values revealed smaller reductions in trend-derived change in O₃ mixing ratios in 2021 since 2000 for the lower τ values compared to higher values in Europe. This, coupled with the fact that generally O₃ trends across Europe are positive, suggesting that the lowest ambient O₃ mixing ratios are increasing more rapidly than the highest values. An
335 assessment of the spatio-temporal distribution of the first and second change points revealed more sites with a directional switch in O₃ trend across Europe were in the positive to negative direction in the first change point, but with more sites with a negative to positive second change point. In the USA dataset, the biggest switches from negative to positive in the first change point occurred in California and Florida, but a reversal of this trend from positive to negative was also observed across these states in the second change point. To supplement this, a calculation of the 4th highest daily maximum 8-hour running mean
340 for O₃ (4MDA8) revealed high 4MDA8 hotspots in parts of southern Europe, but particularly in California, consistent with previous findings of Fleming et al. (2018). In Europe, the vast majority of directionally switching second change points in NO₂ occurred in 2020 in the negative to positive direction. This was attributed to the a COVID-19 effect, whereby ambient NO₂ mixing ratios were lower in 2020, leading to an increasing trend in the subsequent years as business-as-usual conditions resumed. These increasing NO₂ concentrations have in some cases been accompanied by increasing O₃/O_x and should continue
345 to be observed as in many cases the prior downward trend in NO₂ has not resumed.

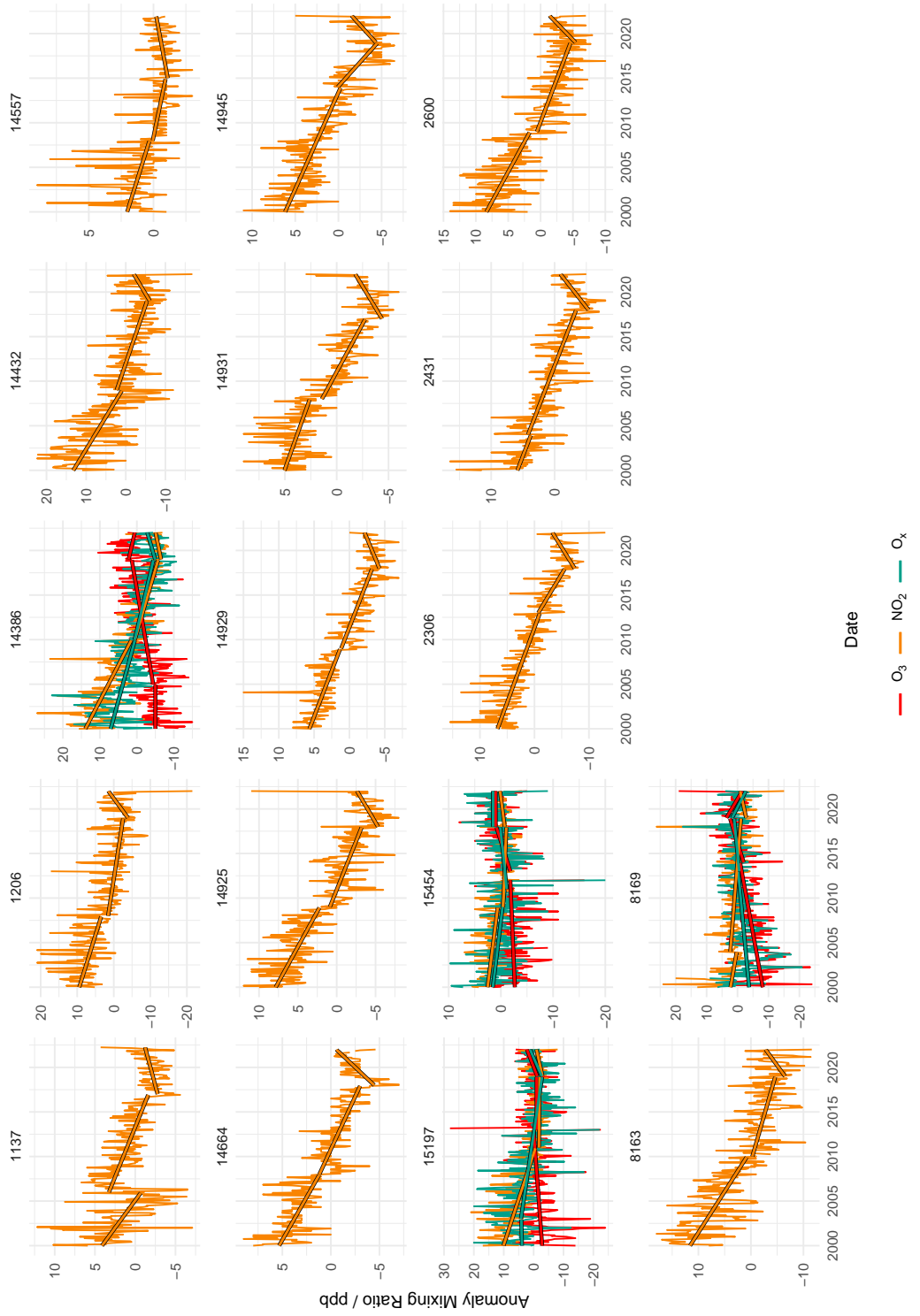


Figure 14. Sites in the USA that had increasing NO_2 since 2015. Monthly averaged O_3 (red), NO_2 (orange) and O_x (green) anomaly are shown. O_3 and O_x trends differ from those presented elsewhere in the manuscript as the piecewise quantile regression where the second change point has been restricted to match that of the NO_2 at each site.

Code and data availability. All data for this study can be downloaded from the relevant databases. Code for performing the download as well as the analysis can be found at 10.5281/zenodo.14538198 (Drysdale and Nelson, 2024)

Author contributions. BSN and WSD equally contributed to all aspects of this manuscript's production

Competing interests. The authors declare that they have no conflict of interest.

350 *Acknowledgements.* The Viking cluster was used during this project, which is a high performance compute facility provided by the University of York. We are grateful for computational support from the University of York, IT Services and the Research IT team.

The Authors acknowledge Prof. James Lee for their scientific advice and Prof. David Carslaw and Dr Stuart Lacy for their advice on the statistical analysis. We also thank Dr Stuart Lacy for their help with SQL and very useful suggestions on managing large datasets.

References

- 355 Berrocal, V., Gelfand, A., and Holland, D.: Assessing exceedance of ozone standards: a space-time downscaler for fourth highest ozone concentrations, *Environmetrics*, 25, 279–291, [https://doi.org/https://doi.org/10.1002/env.2273](https://doi.org/10.1002/env.2273), 2014.
- Chang, K.-L., Schultz, M. G., Koren, G., and Selke, N.: Guidance note on best statistical practices for TOAR analyses, <https://arxiv.org/abs/2304.14236>, 2023.
- Drysdale, W. S.: wacl-york/toarR: v0.1.0, <https://doi.org/10.5281/zenodo.14537446>, 2024.
- 360 Drysdale, W. S. and Nelson, B. S.: wacl-york/Urban-Ozone-Trends-in-Europe-and-the-USA-2000-2021: v0.1.0 preprint, <https://doi.org/10.5281/zenodo.14538198>, 2024.
- Environment Protection Agency: National Ambient Air Quality Standards for Ozone, *Federal Register*, 80, 65 292–65 468, <https://www.epa.gov/ground-level-ozone-pollution/ozone-national-ambient-air-quality-standards-naaqs>, 2015.
- European Environment Agency: Air Quality e-Reporting, <https://www.eea.europa.eu/en/datahub/datahubitem-view/>, a.
- 365 European Environment Agency: EIONET, <https://cdr.eionet.europa.eu/>, b.
- Fleming, Z. L., Doherty, R. M., von Schneidemesser, E., Malley, C. S., Cooper, O. R., Pinto, J. P., Colette, A., Xu, X., Simpson, D., Schultz, M. G., Lefohn, A. S., Hamad, S., Moolla, R., Solberg, S., and Feng, Z.: Tropospheric Ozone Assessment Report: Present-day ozone distribution and trends relevant to human health, *Elementa: Science of the Anthropocene*, 6, 12, <https://doi.org/10.1525/elementa.273>, 2018.
- 370 Grange, S.: Technical note: saqgetr R package, <https://doi.org/10.13140/RG.2.2.15533.44001>, 2019.
- Grange, S. K., Lee, J. D., Drysdale, W. S., Lewis, A. C., Hueglin, C., Emmenegger, L., and Carslaw, D. C.: COVID-19 lockdowns highlight a risk of increasing ozone pollution in European urban areas, *Atmospheric Chemistry and Physics*, 21, 4169–4185, <https://doi.org/10.5194/acp-21-4169-2021>, 2021.
- He, H., Liang, X.-Z., Sun, C., Tao, Z., and Tong, D. Q.: The long-term trend and production sensitivity change in the US ozone pollution from observations and model simulations, *Atmospheric Chemistry and Physics*, 20, 3191–3208, <https://doi.org/10.5194/acp-20-3191-2020>, 2020.
- 375 Jhun, I., Coull, B. A., Zanobetti, A., and Koutrakis, P.: The impact of nitrogen oxides concentration decreases on ozone trends in the USA, *Air Quality, Atmosphere & Health*, 8, 283–292, <https://doi.org/10.1007/s11869-014-0279-2>, 2015.
- Jonson, J. E., Simpson, D., Fagerli, H., and Solberg, S.: Can we explain the trends in European ozone levels?, *Atmospheric Chemistry and Physics*, 6, 51–66, <https://doi.org/10.5194/acp-6-51-2006>, 2006.
- 380 Lee, J. D., Drysdale, W. S., Finch, D. P., Wilde, S. E., and Palmer, P. I.: UK surface NO₂ levels dropped by 42 % during the COVID-19 lockdown: impact on surface O₃, *Atmospheric Chemistry and Physics*, 20, 15 743–15 759, <https://doi.org/10.5194/acp-20-15743-2020>, 2020.
- Malashock, D. A., DeLang, M. N., Becker, J. S., Serre, M. L., West, J. J., Chang, K.-L., Cooper, O. R., and Anenberg, S. C.: Estimates of ozone concentrations and attributable mortality in urban, peri-urban and rural areas worldwide in 2019, *Environmental Research Letters*, 17, 054 023, <https://doi.org/10.1088/1748-9326/ac66f3>, 2022.
- Mills, G., Pleijel, H., Malley, C. S., Sinha, B., Cooper, O. R., Schultz, M. G., Neufeld, H. S., Simpson, D., Sharps, K., Feng, Z., Gerosa, G., Harmens, H., Kobayashi, K., Saxena, P., Paoletti, E., Sinha, V., and Xu, X.: Tropospheric Ozone Assessment Report: Present-day tropospheric ozone distribution and trends relevant to vegetation, *Elementa: Science of the Anthropocene*, 6, 47, <https://doi.org/10.1525/elementa.302>, 2018.

- Schröder, S., Schultz, M. G., Selke, N., Sun, J., Ahring, J., Mozaffari, A., Romberg, M., Epp, E., Lensing, M., Apweiler, S., Leufen, L. H., Betancourt, C., Hagemeier, B., and Rajveer, S.: TOAR Data Infrastructure, <https://doi.org/10.34730/4D9A287DEC0B42F1AA6D244DE8F19EB3>, 2021.
- Shi, Z., Song, C., Liu, B., Lu, G., Xu, J., Vu, T. V., Elliott, R. J. R., Li, W., Bloss, W. J., and Harrison, R. M.: Abrupt
395 but smaller than expected changes in surface air quality attributable to COVID-19 lockdowns, *Science Advances*, 7, eabd6696,
<https://doi.org/10.1126/sciadv.abd6696>, 2021.
- Sillman, S.: Chapter 12 The relation between ozone, NOx and hydrocarbons in urban and polluted rural environments, in: *Air Pollution Science for the 21st Century*, edited by Austin, J., Brimblecombe, P., and Sturges, W., vol. 1 of *Developments in Environmental Science*, pp. 339–385, Elsevier, [https://doi.org/https://doi.org/10.1016/S1474-8177\(02\)80015-8](https://doi.org/https://doi.org/10.1016/S1474-8177(02)80015-8), 2002.
- 400 Sillman, S., Logan, J. A., and Wofsy, S. C.: The sensitivity of ozone to nitrogen oxides and hydrocarbons in regional ozone episodes, *Journal of Geophysical Research: Atmospheres*, 95, 1837–1851, <https://doi.org/https://doi.org/10.1029/JD095iD02p01837>, 1990.
- Sokhi, R. S., Singh, V., Querol, X., Finardi, S., Targino, A. C., de Fatima Andrade, M., Pavlovic, R., Garland, R. M., Massagué, J., Kong, S., Baklanov, A., Ren, L., Tarasova, O., Carmichael, G., Peuch, V.-H., Anand, V., Arbillia, G., Badali, K., Beig, G., Belalcazar, L. C., Bolignano, A., Brimblecombe, P., Camacho, P., Casallas, A., Charland, J.-P., Choi, J., Chourdakis, E., Coll, I., Collins, M., Cyrys, J.,
405 da Silva, C. M., Di Giosa, A. D., Di Leo, A., Ferro, C., Gavidia-Calderon, M., Gayen, A., Ginzburg, A., Godefroy, F., Gonzalez, Y. A., Guevara-Luna, M., Haque, S. M., Havenga, H., Herod, D., Hörrak, U., Hussein, T., Ibarra, S., Jaimes, M., Kaasik, M., Khaiwal, R., Kim, J., Kousa, A., Kukkonen, J., Kulmala, M., Kuula, J., La Violette, N., Lanzani, G., Liu, X., MacDougall, S., Manseau, P. M., Marchegiani, G., McDonald, B., Mishra, S. V., Molina, L. T., Mooibroek, D., Mor, S., Moussiopoulos, N., Murena, F., Niemi, J. V., Noe, S., Nogueira, T., Norman, M., Pérez-Camaño, J. L., Petäjä, T., Piketh, S., Rathod, A., Reid, K., Retama, A., Rivera, O., Rojas, N. Y., Rojas-Quincho,
410 J. P., San José, R., Sánchez, O., Seguel, R. J., Sillanpää, S., Su, Y., Tapper, N., Terrazas, A., Timonen, H., Toscano, D., Tsegas, G., Velders, G. J., Vlachokostas, C., von Schneidemesser, E., VPM, R., Yadav, R., Zalakeviciute, R., and Zavala, M.: A global observational analysis to understand changes in air quality during exceptionally low anthropogenic emission conditions, *Environment International*, 157, 106 818,
<https://doi.org/https://doi.org/10.1016/j.envint.2021.106818>, 2021.
- Szopa, S., Naik, V., Bhupesh, A., Artaxo, P., Berntsen, T., Collins, W. D., Fuzzi, S., Gallardo, L., Kiendler-Scharr, A., Klimont, Z., Liao, H.,
415 Unher, N., and Zanis, P.: *Short-lived Climate Forcers*, p. 817–922, Cambridge University Press, 2021.
- UN: World urbanization prospects 2018 highlights, UN, <http://digitallibrary.un.org/record/3828520>, 2019.
- Yan, Y., Pozzer, A., Ojha, N., Lin, J., and Lelieveld, J.: Analysis of European ozone trends in the period 1995–2014, *Atmospheric Chemistry and Physics*, 18, 5589–5605, <https://doi.org/10.5194/acp-18-5589-2018>, 2018.